ARTICLES
https://doi.org/10.1038/s41566-021-00891-y

nature photonics

Robust, efficient, micrometre-scale phase modulators at visible wavelengths

Guozhen Liang[1,4], Heqing Huang[1,4], Aseema Mohanty[2,3], Min Chul Shin[2], Xingchen Ji[2], Michael Joseph Carter[1], Sajan Shrestha[1], Michal Lipson[2]✉ and Nanfang Yu[1]✉

Optical phase modulators are essential to large-scale integrated photonic systems at visible wavelengths and are promising for many emerging applications. However, current technologies require large device footprints and either high power consumption or high drive voltages, limiting the number of active elements in a visible-spectrum integrated photonic circuit. Here, we demonstrate visible-spectrum silicon nitride thermo-optic phase modulators based on adiabatic micro-ring resonators that offer at least a one-order-of-magnitude reduction in both the device footprint and power consumption compared with waveguide phase modulators. Designed to operate in the strongly over-coupled regime, the micro-resonators provide 1.6π phase modulation with minimal amplitude variations, corresponding to modulation losses as small as 0.61 dB. By delocalizing the resonant mode, the adiabatic micro-rings exhibit improved robustness against fabrication variations: compared with regular micro-rings, less than one-third of the power is needed to thermo-optically align the resonances of the adiabatic micro-rings across the chip to the laser frequency.

Large-scale integration of phase modulators is at the core of photonic systems for on-chip optical routing and free-space wavefront shaping, two fundamental operations that are pivotal to the realization of a diverse range of applications, including optical switching fabrics[1], artificial neural networks[2–4], light ranging and detection[5,6], free-space optical communication[7] and phased-array imaging[8]. Visible-spectrum integrated photonics is another exciting frontier with many emerging applications, such as augmented- and virtual-reality displays[9,10], quantum information processing[11–13], nonlinear optics[14,15], optical sensing[16,17] and optogenetics[18,19]. Massively integrated chip-scale systems in the visible and near-infrared spectral regions demand micrometre-scale phase modulators with low power consumption or drive voltages. These requirements are particularly challenging to meet for visible-spectrum integrated photonics, where the available materials platforms that are compatible with complementary metal–oxide–semiconductor (CMOS) processes (that is, silicon nitride (SiN)[20–27], aluminium nitride (AlN)[14,28,29] and silicon dioxide (SiO_2)[30,31]) have weak thermo-optic (TO) and electro-optic (EO) effects. For example, the TO coefficient of SiN is much smaller than that of silicon[32,33]: waveguide-based SiN TO phase modulators at visible wavelengths are typically hundreds of micrometres in length and require tens of milliwatts of power for π phase modulation[10]. Lithium niobate (LN) is a new materials platform for integrated photonics with ultralow propagation losses[34,35], although it is not CMOS compatible. Given the large EO coefficient of LN, state-of-the-art visible-spectrum LN waveguide phase modulators require a half-wave voltage–length product, $V_\pi L$, of 1.6 V cm (ref. [35]), implying that a device driven by a CMOS-level voltage would be approximately one centimetre in length. Liquid-crystal cladding provides another modulation mechanism with a smaller $V_\pi L$, but it does not support high-speed modulation[36,37].

Conventional phase modulators at visible wavelengths are based on phase accumulation as a result of light propagation in waveguides, which limits large-scale on-chip integration. Modulators based on optical resonance, such as micro-rings[14–17,22–24,28,29,31,32,34,35], micro-discs[1,21] and photonic crystal slabs[13,30] as well as those based on plasmonic confinement[38,39] support enhanced light–matter interactions and can substantially reduce device footprints, power consumption and drive voltages. However, resonators are not widely used for phase modulation because an optical resonance is usually associated with large amplitude modulation[40], and the phase coverage across an optical resonance may be substantially smaller than 2π (ref. [41]). Furthermore, resonant structures are sensitive to fabrication and temperature variations[41], demanding extra power for thermo-optically stabilizing the resonant frequencies of all devices on the chip and aligning them to the laser frequency.

Here, we demonstrate that phase modulation with minimal losses at visible wavelengths can be achieved in optical micro-resonators operating in the strongly over-coupled regime[1,40–44]. The latter is realized by designing an adiabatic micro-ring resonator that supports resonant modes delocalized from the device sidewalls to reduce optical scattering losses, and by choosing a coupler geometry to enhance the resonator–waveguide coupling strength. Our visible-spectrum modulators exhibit a marked reduction in both footprint and power consumption for TO modulation. Delocalization of modes further improves the devices' tolerance to fabrication variations compared with conventional micro-ring resonators and waveguide phase shifters. Our approach can potentially enable large-scale, monolithic integrated photonics at visible wavelengths.

Strongly over-coupled micro-resonators for phase modulation

Phase modulation with minimal losses can be achieved in a device consisting of a micro-resonator coupled to a waveguide and operating in the strongly over-coupled regime (Fig. 1). The latter refers to a condition where the waveguide–resonator coupling rate, γ_e, is at least one order of magnitude larger than the intrinsic decay rate, γ_o, of the resonator, which results from a collective of optical scattering,

[1]Department of Applied Physics and Applied Mathematics, Columbia University, New York, NY, USA. [2]Department of Electrical Engineering, Columbia University, New York, NY, USA. [3]Department of Electrical and Computer Engineering, Tufts University, Medford, MA, USA. [4]These authors contributed equally: Guozhen Liang, Heqing Huang. ✉e-mail: ml3745@columbia.edu; ny2214@columbia.edu

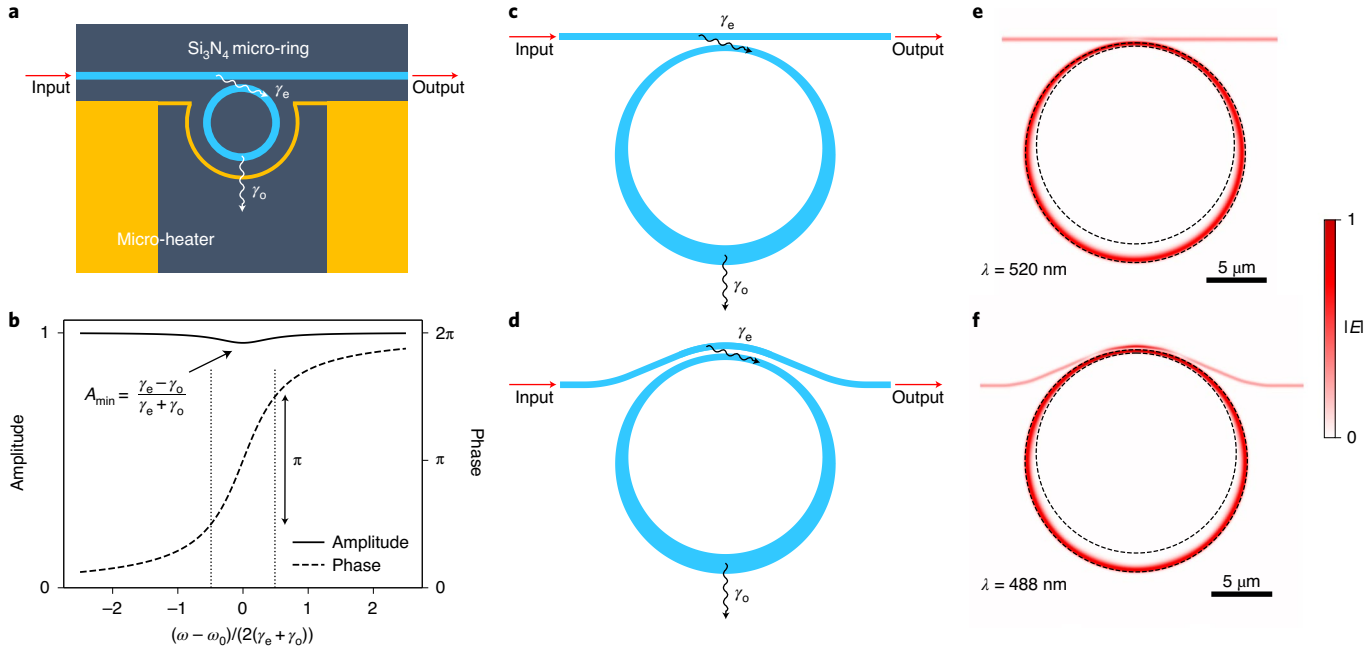

Fig. 1 | Micro-resonator operating in the strongly over-coupled regime for phase modulation. a, Schematic of an optical modulator consisting of a SiN (Si_3N_4) micro-ring resonator coupled to a SiN bus waveguide. Tuning is realized by varying the refractive indices of SiN through the TO effect by using an integrated micro-heater. A device is considered to operate in the strongly over-coupled regime when the coupling rate between the waveguide and the resonator, γ_e, is one order of magnitude larger than the intrinsic decay rate of the resonator, γ_o. **b**, Analytical calculations showing a 2π phase shift with minimal amplitude variations across an optical resonance in the strongly over-coupled regime (assuming $\gamma_e = 50\gamma_o$). Note that the central π phase shift occurs over the linewidth of the resonance $2(\gamma_e + \gamma_o)$ (Supplementary Section 1). ω, source frequency; ω_0, resonant frequency. **c**,**d**, Designs of adiabatic micro-rings operating at the green (**c**) and blue (**d**) wavelengths, respectively. **e**,**f**, Simulated quasi-TE (**e**) and quasi-TM (**f**) resonant modes of the devices in **c** and **d**, respectively, with the dashed curves indicating the device outlines. *E*, electric field strength. In the examples shown in **c**–**f**, the adiabatic micro-rings are defined by two circles displaced from each other: the outer and inner radii are 10 μm and 9 μm, respectively, and the displacement is 0.7 μm, making the narrowest section of the adiabatic ring (at the coupler region) 300 nm in width and the widest section 1.7 μm in width.

absorption and bending losses in the resonator. Operation in the strongly over-coupled regime is ideally suited for phase modulation, as the output signal undergoes a 2π phase shift across an optical resonance, while the optical amplitude, *A*, is minimally affected (Fig. 1b): the amplitude drops to a minimum, A_{min}, of $(\gamma_e - \gamma_o)/(\gamma_e + \gamma_o)$ at the centre of the resonance (Supplementary Section 1); thus, the modulation loss can be reduced to below 1 dB when $\gamma_e > 17\gamma_o$. In addition to providing phase modulation within a compact device footprint, micro-resonators allow for a substantial reduction in the power consumption of TO modulators and in the $V_\pi L$ of EO modulators by a factor of $F/2$, where F is the finesse factor of the resonator, when compared with waveguide-based phase modulators (Supplementary Sections 4 and 5). It is worth noting that two identical micro-resonators operating in the strongly over-coupled regime along the same bus waveguide can provide a total phase modulation of 4π; as such, there is an approximately linear relationship between the central 2π phase shift and the heating power for TO modulation, and a smaller range of heating power is needed for 2π phase modulation compared with single micro-resonators (Supplementary Section 2). Phase modulation using over-coupled resonators has been demonstrated at the telecommunications wavelengths[1,40,45]; however, it has been extremely challenging to realize the concept in the visible spectral range, due to the requirements of ultra-small waveguide–resonator coupling gaps and low optical losses.

We demonstrate visible-spectrum phase modulators operating in the strongly over-coupled regime based on adiabatic micro-rings (Fig. 1c,d). The overall design strategy is to choose the geometry of the micro-resonators, the gap size between the resonator and the waveguide, and the configuration of the coupler, so that γ_e can be increased and γ_o can be decreased to facilitate device operation under the strong over-coupling condition (Supplementary Section 3). The adiabatic micro-ring in Fig. 1c supports the fundamental quasi-transverse-electric (quasi-TE) resonant modes where the electric-field components are polarized primarily in the plane of the chip. To increase γ_e, a small gap (around 100 nm) is used between the micro-ring and the bus waveguide, and the narrow section of the adiabatic ring is chosen to be phase-matched with the bus waveguide. At the wide section of the adiabatic ring, the optical mode is delocalized from the inner sidewall of the ring (Fig. 1e), so that the contribution to γ_o due to scattering at the sidewall roughness, the primary cause of optical losses in our devices (Supplementary Section 3), can be reduced. The rate of change in width between the narrow and wide sections of the resonator is sufficiently low to prevent the resonator from entering into the chaotic operation regime[46]. Adiabatic micro-rings have been previously used to reduce optical scattering by electrodes in silicon near-infrared EO modulators[47].

A micro-ring phase modulator at the blue wavelengths is comparatively harder to realize due to increased Rayleigh scattering by the sidewall roughness at shorter wavelengths. The sidewall scattering can be mitigated by using an adiabatic micro-ring design that supports quasi-transverse-magnetic (quasi-TM) modes (Fig. 1f), which have smaller evanescent components at the device sidewalls compared with quasi-TE modes[41]. The reduced resonator–waveguide coupling as a result of the weakened evanescent fields is compensated for by using a conveyor belt coupler (Fig. 1d). The latter is optimized to reduce optical scattering due to the coupling between the bus waveguide and the adiabatic micro-ring (Supplementary Section 3).

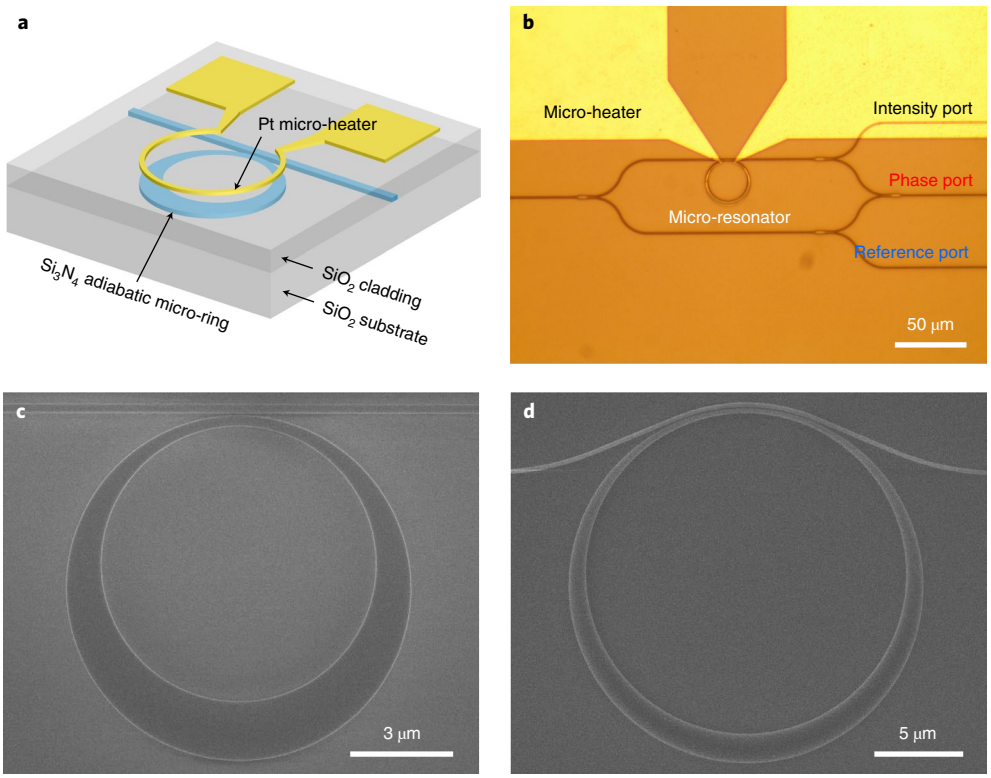

Fig. 2 | Device geometry. a, Schematic of a SiN adiabatic micro-ring with an integrated platinum (Pt) micro-heater. **b**, Microscope image of a device loaded onto one arm of an MZI, which is furnished with three output ports: the 'intensity port' monitors the amplitude response of the micro-ring, the 'reference port' monitors the transmission of the reference waveguide, and the 'phase port' signal is the interference between the micro-ring transmission and the reference signal, allowing for monitoring the phase response of the micro-ring. **c**,**d**, Scanning electron micrographs of the devices (before depositing SiO_2 claddings and adding platinum micro-heaters) working at the green ($\lambda = 530$ nm) (**c**) and blue ($\lambda = 488$ nm) (**d**) wavelengths.

The device designs are demonstrated using the integrated SiN platform, where TO tuning is provided by micro-heaters placed in the close vicinity of the micro-resonators (Fig. 2a). A micro-resonator is loaded on one of the arms of a Mach–Zehnder interferometer (MZI) furnished with three output ports (Fig. 2b) to allow for monitoring the phase and amplitude responses of the resonator across an optical resonance. The frequency of the laser source is initially red-detuned with respect to the resonance; heating up the resonator with the micro-heater leads to increased refractive indices of SiN, and thus a continuous red-shift of the resonance across the laser frequency. If the device operates in the strongly over-coupled regime, the phase of the resonator-loaded arm undergoes a 2π change with minimal amplitude variations across the resonance. This should result in a dip dropping to zero in the output signal from the 'phase port' and a relatively flat output signal from the 'intensity port'; for devices operating in the under-coupled or critical-coupled regime, however, the 'phase port' signal will not drop to zero and the 'intensity port' signal will exhibit large variations (Supplementary Section 6).

Compact, efficient phase modulators in the visible spectral region

Devices working at the green ($\lambda = 530$ nm) and blue ($\lambda = 488$ nm) wavelengths are fabricated using standard cleanroom techniques, including thin-film growth, electron-beam lithography (EBL) and inductively coupled plasma etching (Methods section). The 190-nm-thick SiN device layer is grown by low-pressure chemical vapour deposition. The plasma etching recipe is optimized to reduce roughness on the vertical sidewalls, and chemical mechanical polishing is used to reduce roughness on the top surfaces of the SiN micro-rings. An optical microscope image and scanning electron micrographs of the fabricated devices are shown in Fig. 2.

Figure 3a,b shows, respectively, measured 'intensity' and 'phase' port signals and extracted amplitude and phase responses of an adiabatic micro-ring resonator with an outer radius of $R = 10\,\mu$m as a function of the micro-heater power at $\lambda = 530$ nm. Across the resonance, the phase changes by approximately 1.6π when the heating power changes by ~4 mW; near the centre of the resonance, the phase changes by π when the heating power changes by only ~0.85 mW; meanwhile, the output from the intensity port changes minimally by 0.87 dB (corresponding to an amplitude variation of ~10%). The intrinsic and loaded quality factors (Q factors) of the adiabatic micro-ring are estimated to be 2.1×10^5 and 1.0×10^4, respectively (Supplementary Section 9). For control devices based on straight SiN waveguides with a length ranging from 200 to 500 μm, a heating power of ~20 mW is required to achieve a π phase shift (Fig. 3e and Supplementary Section 10). In comparison, our adiabatic micro-ring device with a diameter of 20 μm requires less than 1 mW for π phase modulation, representing a reduction of heating power by a factor greater than 20. This agrees with our theoretical analysis that micro-resonators offer a reduction of power consumption in TO modulation by a factor of $F/2$, where F is approximately 46 in our experimentally demonstrated device (Supplementary Section 9).

We also experimentally demonstrate phase modulators at the green wavelength based on micro-disc resonators with conveyer belt couplers (Supplementary Section 8). Operating at the fundamental whispering gallery mode (WGM), these devices can exhibit slightly reduced power consumption compared with adiabatic micro-rings at $\lambda = 530$ nm: the best of them requires a heating power change of 0.68 mW for π phase modulation, with a modulation loss of 1.13 dB and a finesse factor of $F = 71$ (Supplementary Fig. 9). However, the micro-disc devices typically operate under a multimodal condition

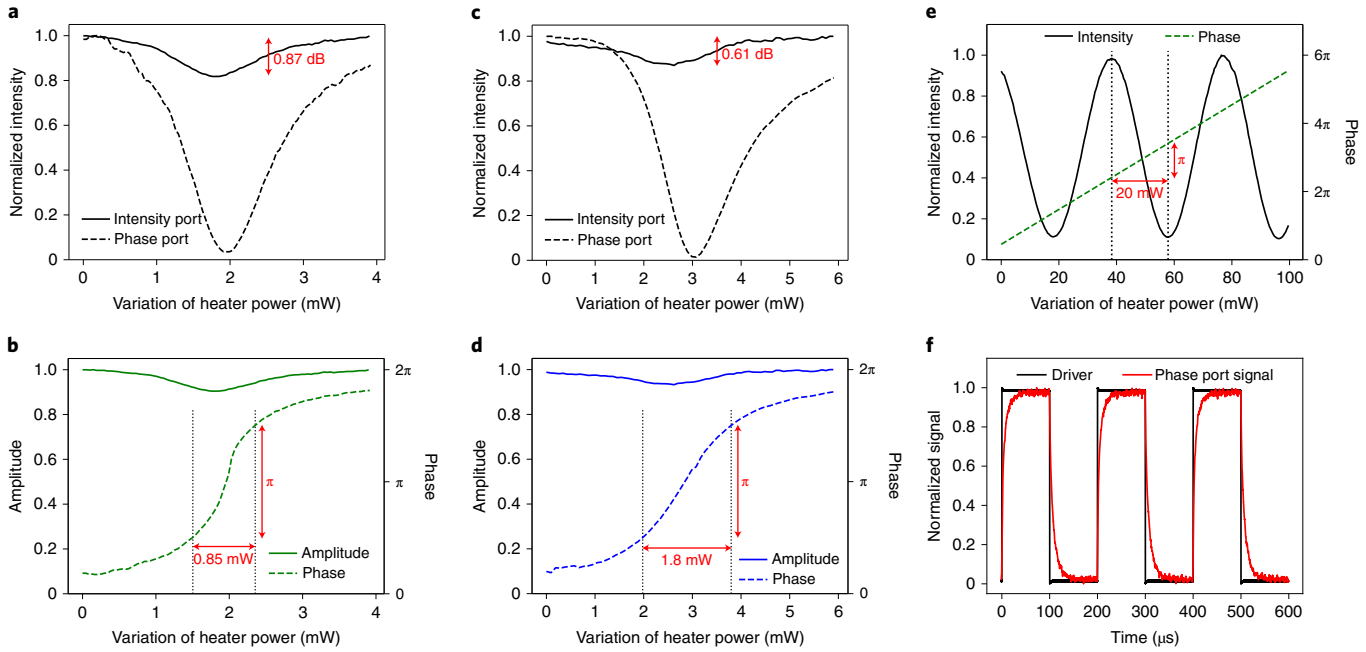

Fig. 3 | Experimental demonstration of phase modulation with minimal amplitude variations at visible wavelengths. a–**d**, Measured signals from the 'intensity' and 'phase' ports and extracted amplitude and phase responses of an adiabatic micro-ring resonator with a 10 μm radius at $\lambda = 530$ nm (**a** and **b**), and an adiabatic micro-ring resonator with a 10 μm radius at $\lambda = 488$ nm (**c** and **d**). The asymmetry of the resonance dip in the 'phase port' signals in **a** and **c** is due to a slight imbalance between the two arms of the integrated MZI. **e**, Normalized transmission response of an MZI control device consisting of straight 200 μm waveguides at $\lambda = 530$ nm and the extracted phase response. **f**, Measured signal at the 'phase port' of an adiabatic micro-ring resonator at $\lambda = 488$ nm, as well as the drive voltage applied to the micro-heater.

and their higher-order WGMs may not necessarily operate in the strongly over-coupled regime (Supplementary Fig. 9).

Phase modulation with minimal variation of the amplitude at the blue wavelength is also demonstrated experimentally. A heating power change of 1.8 mW is needed for a π phase shift (Fig. 3d) and the modulation loss is as low as 0.61 dB (Fig. 3c). The estimated intrinsic and loaded Q factors are 1.1×10^5 and 3.5×10^3, respectively, and the finesse factor, F, is approximately 14. The slightly increased power consumption compared with the devices at the green wavelength is due to the decreased F and a reduced modal overlap between the quasi-TM modes and the SiN micro-resonators.

We also experimentally demonstrate strongly over-coupled SiN micro-rings at telecommunications wavelengths, showing that phase tuning with a small modulation loss of 0.61 dB can be achieved in devices with a radius of 15 μm and a finesse factor of $F = 26$ (Supplementary Section 16). A comparison between our visible-spectrum and telecommunications micro-rings and optimized serpentine waveguide phase shifters[48,49] shows that our devices have a clear advantage in terms of power efficiency, compactness and small loss (Supplementary Section 17). In Supplementary Section 15, we further demonstrate, using realistic propagation losses of foundry-fabricated SiN waveguides[27] in full-wave simulations, that a suitably designed adiabatic micro-ring can support a plethora of resonances across the entire visible spectrum, all satisfying the strong over-coupling condition, and thus can function as a versatile phase shifter with minimal modulation losses in the visible spectrum (that is, below 0.3 dB in the green and red region and below 1 dB in the blue region).

The modulation speed of the visible-spectrum devices is measured by applying a square wave to the micro-heater and monitoring the output from the 'phase port' of the MZI. Figure 3f shows the measured drive voltage and output signal of an adiabatic micro-ring device at the blue wavelength. The device response time, calculated by fitting the rising and falling edges of the output signal with an exponential function and extracting the time constant, is 3.4 ± 1.2 μs ($n = 8$ devices) (Supplementary Section 11), which corresponds to a modulation frequency of ~290 kHz. The response time of control waveguide phase modulators fabricated on the same chip is found to be similar (3.9 ± 0.6 μs, for $n = 6$ devices). The measured response time is in good agreement with that of thermodynamic simulations (Supplementary Section 11). The simulations further show that the local peak temperature of the waveguide devices is at least 30 °C higher than that of the micro-resonators (Supplementary Fig. 11).

Robust performance against fabrication variations

Compared with conventional micro-ring resonators, adiabatic micro-rings are robust against fabrication variations, such as the sidewall roughness and systematic variations of the ring geometry[44,50] (Supplementary Section 13). The optical mode at the wide section of the adiabatic micro-ring has a reduced overlap with the sidewalls; therefore, optical scattering losses become insensitive to variations in the degree of sidewall roughness, resulting in a substantially reduced and more consistent γ_o value. In addition, delocalization of modes at the wide section of the adiabatic micro-ring makes the modal refractive index insensitive to the variation of the waveguide width (Supplementary Fig. 12), which helps to stabilize the resonant frequency.

We carried out a comparative study of 52 adiabatic micro-ring devices and 49 regular micro-ring devices fabricated on the same chip at $\lambda = 488$ nm. The two types of device have the same outer radius and coupler geometry except that the regular micro-rings have a constant waveguide width, which is equal to that of the narrowest section of the adiabatic micro-rings (inset of Fig. 4a). For the regular micro-rings the histogram of γ_o/γ_e (that is, decay rate/

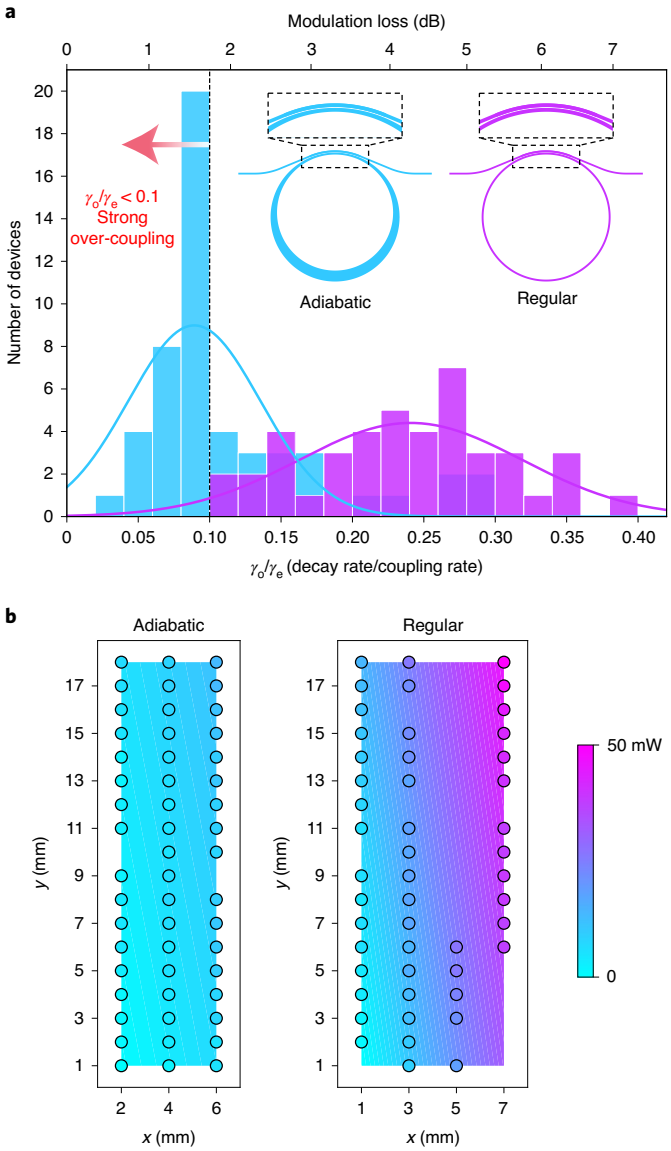

Fig. 4 | Robustness of adiabatic micro-rings against fabrication variations. **a**, Histograms of γ_o/γ_e (decay rate/coupling rate) and the corresponding modulation loss of adiabatic and regular micro-rings fabricated on the same chip at $\lambda = 488$ nm. Note that none of the regular micro-rings satisfy the strong over-coupling condition ($\gamma_o/\gamma_e < 0.1$), whereas 63% of the adiabatic micro-rings operate in the strongly over-coupled regime. The modulation loss of the 52 adiabatic micro-rings is 2.0 ± 1.1 dB. The minimum and median of the modulation loss are 0.61 dB and 1.62 dB, respectively. The percentage of devices with a modulation loss of <1 dB is 7.7%. Normal distribution fittings are plotted as solid curves. Inset: geometry of the two types of device. **b**, Measured heating power to align the device resonant wavelength to the laser wavelength ($\lambda = 488$ nm) as a function of the device location (x,y), with adiabatic and regular micro-rings occupying alternate columns on the same chip. Measured data are plotted in circles (the absence of circles corresponds to devices with damaged facets that prevent efficient light coupling and characterization), and the background is a linear regression fit to the data.

coupling rate) peaks at 0.24 (corresponding to a relatively large modulation loss of 4.2 dB) with a standard deviation of 0.078, whereas for the adiabatic micro-rings the histogram of γ_o/γ_e peaks at a much smaller value of 0.09 (corresponding to a modulation loss of 1.5 dB) and also has a smaller standard deviation of 0.046 (Fig. 4a). With γ_e being similar in the two types of device, the experimental results indicate that the decay rate, γ_o, of the adiabatic micro-ring is approximately one-third of that of the regular micro-ring. The magnitude and variation of γ_o can be further reduced by leveraging advanced facilities in semiconductor fabrication foundries.

Figure 4b shows the spatial distribution of the heating power required to align the centre of the resonance to the laser frequency for both types of devices on the chip. Across an area of $\Delta x \approx 6$ mm and $\Delta y \approx 17$ mm on the chip, the heating power of the regular micro-rings exhibits a gradient of 5.44 mW mm^{-1}, whereas that of the adiabatic micro-rings is only 1.60 mW mm^{-1}. This variation of heating power is caused by a systematic variation of the SiN growth and etching conditions across the chip, resulting in a variation of the SiN layer thickness and waveguide width (Supplementary Section 12). Our results demonstrate the enhanced robustness of the adiabatic micro-rings against such systematic variations, with the consequence that the heating power required for aligning the resonances of the adiabatic micro-rings across the chip to the laser frequency can be reduced by more than a factor of three compared with that of the regular micro-rings. In Supplementary Section 13 we further show that the variation of the effective modal index induced by a systematic variation of the device geometry and the resulting phase error are small in adiabatic micro-rings compared with waveguide phase shifters.

Discussion and conclusion

The work takes a concrete step beyond the concept of over-coupling by developing a set of design strategies to reach the strong over-coupling extreme in the most difficult portion of the visible spectrum (that is, short wavelengths in the visible region). It proposes and experimentally implements adiabatic micro-rings operating under the strong over-coupling condition to provide phase modulation with optical losses that are substantially less than 1 dB (for example, 0.6 dB in the blue spectral range); it also theoretically demonstrates that a suitably designed adiabatic micro-ring can operate in the strongly over-coupled regime over the entire visible spectrum, and thus can be used as a phase shifter for light of any colour in the visible region. The adiabatic micro-rings demonstrate a clear advantage in terms of power efficiency and compactness compared with straight and serpentine waveguide devices. The proposed devices can also help to address the issue of phase error induced by systematic material growth and fabrication variations, a prevalent and consistent challenge in large-scale integrated photonic circuits. These compact, efficient and robust visible-spectrum phase modulators will be most suitable for highly integrated systems with small size, weight and power consumption (SWaP), such as in augmented- and virtual-reality goggles, quantum information processing circuits, optical artificial neural networks and neural probes for optogenetics.

The design strategies employed for our visible-spectrum TO devices can be applied to EO modulators to reduce the $V_\pi L$, and can be adapted in other spectral ranges (for example, ultraviolet, telecommunications, mid-infrared and terahertz ranges) and in other resonator designs (for example, photonic crystal cavities and inversely designed optical resonators). Thus, our work can inspire future efforts where people will implement strong over-coupling in a wide range of resonator-based devices to enhance light–matter interactions (for example, for controlling group delay and for enhancing optical nonlinearity), while suppressing optical losses at the same time.

The possible disadvantages of using resonator-based phase modulators include (1) an upper bound of the modulation frequency that is inversely proportional to the loaded Q factor, (2) the introduction of true time delay and distortion to short optical pulses due to group delay and group velocity dispersion of the resonance, (3) modulation losses, that is, not a perfectly constant amplitude response, and (4) thermal bias needed to tune a resonance to the laser frequency and caution needed to maintain the stability of the laser frequency. The first two disadvantages are, however, not likely

to limit applications in the visible region, which, unlike telecommunications, typically do not require an ultrahigh modulation speed (for example, optogenetic probes just need to be much faster than the firing of a neuron; the refresh rate of an augmented-reality display just needs to be faster than the perception of the human eye). The modulation loss can be minimized by pushing devices deeper into the strongly over-coupled regime. The thermal bias required for tuning a micro-ring resonance can be reduced by using rings of larger radius (a smaller free spectral range).

Online content

Any methods, additional references, Nature Research reporting summaries, source data, extended data, supplementary information, acknowledgements, peer review information; details of author contributions and competing interests; and statements of data and code availability are available at https://doi.org/10.1038/s41566-021-00891-y.

Received: 22 September 2020; Accepted: 8 September 2021;
Published online: 22 November 2021

References

1. Haffner, C. et al. Nano–opto-electro-mechanical switches operated at CMOS-level voltages. *Science* **366**, 860–864 (2019).
2. Tait, A. N., Nahmias, M. A., Shastri, B. J. & Prucnal, P. R. Broadcast and weight: an integrated network for scalable photonic spike processing. *J. Lightwave Technol.* **32**, 4029–4041 (2014).
3. Shen, Y. et al. Deep learning with coherent nanophotonic circuits. *Nat. Photon.* **11**, 441–446 (2017).
4. Zhang, Q., Yu, H., Barbiero, M., Wang, B. & Gu, M. Artificial neural networks enabled by nanophotonics. *Light Sci. Appl.* **8**, 42 (2019).
5. Sun, J., Timurdogan, E., Yaacobi, A., Hosseini, E. S. & Watts, M. R. Large-scale nanophotonic phased array. *Nature* **493**, 195–199 (2013).
6. Aflatouni, F., Abiri, B., Rekhi, A. & Hajimiri, A. Nanophotonic projection system. *Opt. Express* **23**, 21012–21022 (2015).
7. Guan, B. et al. Free-space coherent optical communication with orbital angular, momentum multiplexing/demultiplexing using a hybrid 3D photonic integrated circuit. *Opt. Express* **22**, 145–156 (2014).
8. Clevenson, H. A. et al. Incoherent light imaging using an optical phased array. *Appl. Phys. Lett.* **116**, 031105 (2020).
9. Raval, M., Yaacobi, A. & Watts, M. R. Integrated visible light phased array system for autostereoscopic image projection. *Opt. Lett.* **43**, 3678–3681 (2018).
10. Shin, M. C. et al. Chip-scale blue phased array. *Opt. Lett.* **45**, 1934–1937 (2020).
11. Mehta, K. K. et al. Integrated optical addressing of an ion qubit. *Nat. Nanotechnol.* **11**, 1066–1070 (2016).
12. Sipahigil, A. et al. An integrated diamond nanophotonics platform for quantum optical networks. *Science* **354**, 847–850 (2016).
13. Burgers, A. P. et al. Clocked atom delivery to a photonic crystal waveguide. *Proc. Natl Acad. Sci. USA* **116**, 456–465 (2019).
14. Xiong, C. et al. Aluminum nitride as a new material for chip-scale optomechanics and nonlinear optics. *New J. Phys.* **14**, 095014 (2012).
15. Moss, D. J., Morandotti, R., Gaeta, A. L. & Lipson, M. New CMOS-compatible platforms based on silicon nitride and Hydex for nonlinear optics. *Nat. Photon.* **7**, 597–607 (2013).
16. Armani, A. M., Kulkarni, R. P., Fraser, S. E., Flagan, R. C. & Vahala, K. J. Label-free, single-molecule detection with optical microcavities. *Science* **317**, 783–787 (2007).
17. Zhu, J. et al. On-chip single nanoparticle detection and sizing by mode splitting in an ultrahigh-Q microresonator. *Nat. Photon.* **4**, 46–49 (2010).
18. Hoffman, L. et al. Low loss CMOS-compatible PECVD silicon nitride waveguides and grating couplers for blue light optogenetic applications. *IEEE Photon. J.* **8**, 2701211 (2016).
19. Mohanty, A. et al. Reconfigurable nanophotonic silicon probes for sub-millisecond deep-brain optical stimulation. *Nat. Biomed. Eng.* **4**, 223–231 (2020).
20. Gorin, A., Jaouad, A., Grondin, E., Aimez, V. & Charette, P. Fabrication of silicon nitride waveguides for visible-light using PECVD: a study of the effect of plasma frequency on optical properties. *Opt. Express* **16**, 13509–13516 (2008).
21. Hosseini, E. S., Yegnanarayanan, S., Atabaki, A. H., Soltani, M. & Adibi, A. High quality planar silicon nitride microdisk resonators for integrated photonics in the visible wavelength range. *Opt. Express* **17**, 14543–14551 (2009).
22. Gondarenko, A., Levy, J. S. & Lipson, M. High confinement micron-scale silicon nitride high Q ring resonator. *Opt. Express* **17**, 11366–11370 (2009).
23. Tien, M.-C. et al. Ultra-high quality factor planar Si_3N_4 ring resonators on Si substrates. *Opt. Express* **19**, 13551–13556 (2011).
24. Luke, K., Dutt, A., Poitras, C. B. & Lipson, M. Overcoming Si_3N_4 film stress limitations for high quality factor ring resonators. *Opt. Express* **21**, 22829–22833 (2013).
25. Romero-García, S., Merget, F., Zhong, F., Finkelstein, H. & Witzens, J. Silicon nitride CMOS-compatible platform for integrated photonics applications at visible wavelengths. *Opt. Express* **21**, 14036–14046 (2013).
26. Subramanian, A. Z. et al. Low-loss singlemode PECVD silicon nitride photonic wire waveguides for 532–900 nm wavelength window fabricated within a CMOS pilot line. *IEEE Photon. J.* **5**, 2202809 (2013).
27. Sacher, W. D. et al. Visible-light silicon nitride waveguide devices and implantable neurophotonic probes on thinned 200 mm silicon wafers. *Opt. Express* **27**, 37400–37418 (2019).
28. Xiong, C., Pernice, W. H. P. & Tang, H. X. Low-Loss, silicon integrated, aluminum nitride photonic circuits and their use for electro-optic signal processing. *Nano Lett.* **12**, 3562–3568 (2012).
29. Lu, T.-J. et al. Aluminum nitride integrated photonics platform for the ultraviolet to visible spectrum. *Opt. Express* **26**, 11147–11160 (2018).
30. Gong, Y. & Vučković, J. Photonic crystal cavities in silicon dioxide. *Appl. Phys. Lett.* **96**, 031107 (2010).
31. Lee, S. H. et al. Towards visible soliton microcomb generation. *Nat. Commun.* **8**, 1295 (2017).
32. Arbabi, A. & Goddard, L. L. Measurements of the refractive indices and thermo-optic coefficients of Si_3N_4 and SiO_x using microring resonances. *Opt. Lett.* **38**, 3878–3881 (2013).
33. Komma, J., Schwarz, C., Hofmann, G., Heinert, D. & Nawrodt, R. Thermo-optic coefficient of silicon at 1550 nm and cryogenic temperatures. *Appl. Phys. Lett.* **101**, 041905 (2012).
34. Zhang, M., Wang, C., Cheng, R., Shams-Ansari, A. & Lončar, M. Monolithic ultra-high-Q lithium niobate microring resonator. *Optica* **4**, 1536–1537 (2017).
35. Desiatov, B., Shams-Ansari, A., Zhang, M., Wang, C. & Lončar, M. Ultra-low-loss integrated visible photonics using thin-film lithium niobate. *Optica* **6**, 380–384 (2019).
36. Pfeifle, J., Alloatti, L., Freude, W., Leuthold, J. & Koos, C. Silicon-organic hybrid phase shifter based on a slot waveguide with a liquid-crystal cladding. *Opt. Express* **20**, 15359–15376 (2012).
37. Notaros, M., Raval, M., Notaros, J. & Watts, M. R. Integrated visible-light liquid-crystal phase modulator. In *Proc. Frontiers in Optics/Laser Science* FW6B.5 (Optical Society of America, 2018).
38. Dennis, B. S. et al. Compact nanomechanical plasmonic phase modulators. *Nat. Photon.* **9**, 267–273 (2015).
39. Melikyan, A. et al. High-speed plasmonic phase modulators. *Nat. Photon.* **8**, 229–233 (2014).
40. Heebner, J. E., Wong, V., Schweinsberg, A., Boyd, R. W. & Jackson, D. J. Optical transmission characteristics of fiber ring resonators. *IEEE J. Quantum Electron.* **40**, 726–730 (2004).
41. Bogaerts, W. et al. Silicon microring resonators. *Laser Photon. Rev.* **6**, 47–73 (2012).
42. Lee, H., Kananen, T., Soman, A. & Gu, T. Influence of surface roughness on microring-based phase shifters. *IEEE Photon. Technol. Lett.* **31**, 813–816 (2019).
43. Liang, G. et al. Micron-scale, efficient, robust phase modulators in the visible. In *Proc. Conference on Lasers and Electro-Optics* JTh5B.4 (Optical Society of America, 2019).
44. Huang, H. et al. Robust miniature pure-phase modulators at $\lambda = 488$ nm. In *Proc. Conference on Lasers and Electro-Optics* STh1J.4 (Optical Society of America, 2020).
45. Pu, M. et al. Widely tunable microwave phase shifter based on silicon-on-insulator dual-microring resonator. *Opt. Express* **18**, 6172–6182 (2010).
46. Hackenbroich, G. & Nöckel, J. U. Dynamical tunneling in optical cavities. *Europhys. Lett.* **39**, 371–376 (1997).
47. Biberman, A., Timurdogan, E., Zortman, W. A., Trotter, D. C. & Watts, M. R. Adiabatic microring modulators. *Opt. Express* **20**, 29223–29236 (2012).
48. Chung, S., Nakai, M. & Hashemi, H. Low-power thermo-optic silicon modulator for large-scale photonic integrated systems. *Opt. Express* **27**, 13430–13459 (2019).
49. Idres, S. & Hashemi, H. Low-power SiN thermo-optic phase modulator operating in red visible wavelength range. In *Proc. Conference on Lasers and Electro-Optics* JTh2B.7 (Optical Society of America, 2020).
50. Mikkelsen, J. C., Sacher, W. D. & Poon, J. K. S. Adiabatically widened silicon microrings for improved variation tolerance. *Opt. Express* **22**, 9659–9666 (2014).

Methods

Device fabrication. SiN thin films of 190 nm thickness are grown via low-pressure chemical vapour deposition on top of a 2-μm-thick SiO_2 layer on a silicon wafer. The top surface of the SiN layer is polished using chemical–mechanical planarization to reduce the root-mean-squared roughness to ~0.1 nm. The wafer is rinsed using an adhesion promoter (SurPass 3000), then a ~300 nm-thick layer of electron-beam resist (ma-N 2403) is spin coated and baked at 90 °C. EBL (Elionix ELS-G100) is then carried out at 100 keV and 500 pA using a four-pass exposure, with a dose of 500 μC cm^{-2} and appropriate proximity effect corrections (BEAMER) to define the waveguides and resonators. A solution of tetramethylammonium hydroxide in water (AZ 300 MIF) is used to develop the exposed resist. The device pattern written via EBL is transferred into the SiN layer by inductively coupled plasma etching (Oxford PlasmaPro System 100). The excess resist is stripped using a bath of *N*-methyl-2-pyrrolidone (Remover PG) at 80 °C for 2 h. The patterned SiN layer is then cladded with a ~700 nm layer of SiO_2 grown via plasma-enhanced chemical vapour deposition. During a second EBL process to create the micro-heaters, a double layer of poly(methyl methacrylate) is spin coated and baked at 180 °C to serve as an electron-beam resist. EBL is carried out at 100 keV and 20 nA, with a base dose of 800 μC cm^{-2} and appropriate proximity effect corrections. A 3:1 mixture of isopropyl alcohol:deionized water is used to develop the exposed resist. A thin layer of titanium/platinum (of thickness ~10 nm/~100 nm, respectively) is deposited using sputter deposition, and the excess resist is stripped using a bath of Remover PG at room temperature for 24 h.

Device testing. Green light at $\lambda \approx 530$ nm is produced by frequency doubling of a near-infrared tunable diode laser, and is then coupled into the device being tested using free-space optics. Blue light at $\lambda = 488$ nm is produced using a fixed-wavelength diode laser, and is coupled into the device being tested using an optical fibre. An aperture is used to select the signal from one of the three output ports of each device (that is, the intensity, phase and reference ports), and the signal is measured using an avalanche photodiode while tuning the heating power applied to the TO device. The experimental set-up for device characterization is detailed in Supplementary Section 7.

Data availability

The main data supporting the results in this study are available within the paper and its Supplementary Information. The raw datasets generated during the study are too large to be publicly shared, but they are available from the corresponding authors upon reasonable request.

Code availability

The codes used for conducting full-wave simulations of the adiabatic micro-rings and for acquiring data from integrated photonic chips are available from M.L. and N.Y. upon reasonable request.

Acknowledgements

This work was supported by the Defense Advanced Research Projects Agency (grant no. HR00111720034 (G.L., A.M., M.C.S., X.J., M.L. and N.Y.)), the National Science Foundation (grant no. QII-TAQS-1936359 (H.H. and N.Y.) and no. ECCS-2004685 (S.S. and N.Y.)) and the Air Force Office of Scientific Research (grant no. FA9550-14-1-0389 (S.S. and N.Y.) and no. FA9550-16-1-0322 (N.Y.)). A.M. is supported by a Clare Boothe Luce Professorship from the Henry Luce Foundation. M.C.S. acknowledges the support of the 2020 Facebook Fellowship award. M.J.C. is supported by the 2018 SMART Scholarship Program of the US Department of Defense. Device fabrication was carried out at the Columbia Nano Initiative cleanroom, at the Advanced Science Research Center NanoFabrication Facility at the Graduate Center of the City University of New York and at the Cornell NanoScale Science and Technology Facility.

Author contributions

G.L., H.H. and N.Y. conceived the experiments. G.L. and H.H. conducted analytical calculations and full-wave simulations to design the phase modulators. M.J.C. conducted thermodynamic simulations. G.L., H.H., A.M., X.J. and S.S. fabricated the devices. G.L., H.H., A.M., M.C.S. and N.Y. constructed the experimental set-up and characterized device performance. G.L., H.H. and M.J.C. analysed the data. M.L. and N.Y. supervised the project. All authors prepared and edited the manuscript.

Competing interests

G.L., H.H., M.L. and N.Y. are listed as inventors in a US non-provisional patent application no. 16/838,714, which is related to the technology reported in this article and claims priority to US provisional applications no. 62/838,084 and 62/828,261 filed by Columbia University. The remaining authors declare no competing interests.

Additional information

Supplementary information The online version contains supplementary material available at https://doi.org/10.1038/s41566-021-00891-y.

Correspondence and requests for materials should be addressed to Michal Lipson or Nanfang Yu.

Peer review information *Nature Photonics* thanks the anonymous reviewers for their contribution to the peer review of this work.